Phase-field simulation of 2-D Ostwald ripening in the high volume fraction regime

Danan Fan [1,a], S.P. Chen [b], Long-Qing Chen [c,*], P.W. Voorhees [d]

[a] *P.O. Box 5800, MS 1411, Sandia National Laboratories, Albuquerque, NM 87185, USA*
[b] *Theoretical Division, MS B262, Los Alamos National Laboratory, Los Alamos, NM 87545, USA*
[c] *Department of Materials Science and Engineering, The Pennsylvania State University, University Park, PA 16802, USA*
[d] *Department of Materials Science and Engineering, Northwestern University, Evanston, IL 60208, USA*

Abstract

The microstructural evolution and kinetics of Ostwald ripening were studied in the high volume fraction regime by numerically solving the time-dependent Ginzburg–Landau (TDGL) and Cahn–Hilliard equations. It is shown that the growth exponent m is equal to 3, independent of the volume fraction, and the kinetic coefficient k increases as the volume fraction increases. The shape of size distributions changes significantly with increasing volume fraction of the coarsening phase; the skewness changes continuously from negative to positive while the kurtosis decreases in the low fraction regime and increases in the high volume fraction regime. © 2002 Acta Materialia Inc. Published by Elsevier Science Ltd. All rights reserved.

Keywords: Phase transformations; Ostwald ripening; Phase field models

1. Introduction

Ostwald ripening is a process related to the coarsening of one phase dispersed in the matrix of another. The average size of the particles of the dispersed phase increases during coarsening due to diffusion through the matrix phase, and their total number decreases. Modern theories of Ostwald ripening are based on the classical work of Lifshitz,

Slyozov and Wagner [1,2], which is known as LSW theory. In LSW theory, the problem of coarsening kinetics was modeled by assuming a steady-state diffusion field, an infinitesimally dilute second phase, spherical particles and by assuming that particles interact only indirectly with each other through a mean field provided by the matrix.

The LSW theory predicts that during diffusion controlled coarsening the average particle size should increase as a power law in time, $R_t^m - R_0^m = kt$, with an exponent, $m = 3$ and a particle size distribution function that, when scaled by the average particle size, is time independent. These predictions hold rigorously in the limit $t \to \infty$. Since interparticle diffusional interactions are neglected

---

* Corresponding author. Tel.: +1-814-863-8101; fax: +1-814-865-0016.
  E-mail address: chen@ems.psu.edu (L.-Q. Chen).
[1] Present address: Energizer, 25225 Detroit Road, P.O. Box 450777, Westlake, OH 44145, USA.

in LSW theory, this theory is valid only in the physically unrealistic limit of zero volume fraction of the second phase. This is one of the reasons used to explain the disagreement in the size distribution functions measured experimentally [3] and those predicted from the LSW theory.

A variety of techniques have been used to incorporate the effect of finite volume fractions on coarsening, including statistical mechanical theories, mean field theories and numerical simulations [4–13] for three-dimensional (3-D) and [14–20] for two-dimensional (2-D) systems. Despite the different physical bases of these models and theories, most of them assume that the coarsening particles are spherical in shape to avoid the complexity of irregular geometry. However, this assumption cannot remain valid at sufficiently high volume fractions, where the particles within the microstructure become constrained geometrically and exhibit shape accommodation. Shape accommodation results in the non-uniform distribution of curvature along the particle interface. At very high volume fractions of coarsening particles, crowded particles develop flattened sides, curved edges and rounded vertices or corners. This shape accommodation can occur strictly as a result of interparticle diffusional interactions [21]; stresses generated at particle contacts are not necessary to develop flat interfaces [22]. The effects of geometrical complexity present at high volume fractions in systems with sufficient number of particles to determine the evolution of the average particle size have not been included in the theoretical treatments. As a result, the dynamics of Ostwald ripening in the high volume fraction regime remains poorly understood. Since Ostwald ripening is a moving boundary problem, it is very difficult to solve analytically in the high volume fraction regime.

Experimentally, however, testing of the theories describing the effects of volume fractions of coarsening phase on the kinetics of Ostwald ripening is quite difficult to perform. Despite the fact that an increase in the kinetic coefficient k with increasing volume fraction of the coarsening phase has been demonstrated by many experiments [23–27], a variety of growth exponent values m ranging from 2 to 8 have been reported [28–32]. Recently a series of careful experiments on coarsening in solid–liquid systems have been performed [33]. These experiments show that the time required to reach the asymptotic coarsening state predicted by LSW can be quite long. It was never attained in the time-scale of the experiments. This difficulty will also be present in simulations of the coarsening process. If the growth exponent m indeed ultimately varies with volume fraction, then a kinetic coefficient calculated using the classical LSW exponent becomes questionable at high volume fractions.

The purpose of this paper is to study the effect of volume fraction on the Ostwald ripening behavior in 2-D by employing a phase field formulation. The authors have used similar methodologies to study grain growth in single-phase systems [34,35] and the microstructural evolution in two-phase polycrystalline materials [36–39]. Computer simulations using this model allow one not only to monitor the detailed temporal microstructure evolution during Ostwald ripening but also to obtain all the information about the average grain size and size distributions. We will focus on the high volume fraction regime where analytical theories have the most difficulty. The dependencies of growth exponent m, kinetic coefficient k and shapes of size distributions on the volume fractions of the coarsening phase will be systematically examined.

2. The phase field model

The details of this numerical model have been reported in another publication [40]. A schematic microstructure of particles of one phase dispersed in the continuous matrix of another is shown in Fig. 1. In this microstructure, the solubilities or equilibrium concentrations are C_α and C_β for the matrix phase and second phase, respectively. We define a set of continuous field variables,

$$\eta_1(r), \eta_2(r), ..., \eta_p(r), C(r)$$

where p is the number of possible orientations of the second phase grains in space, η_i ($i = 1, ..., p$) are orientation field variables with each orientation field representing grains of a given crystallographic orientation in space, and r is the position in space. These variables change continuously in space and
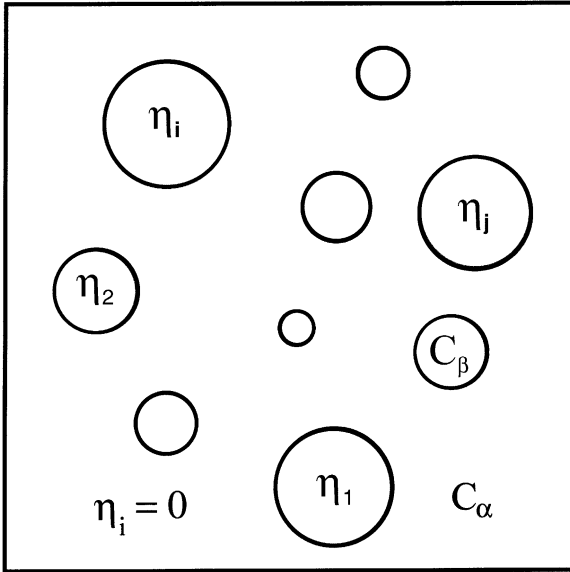
Fig. 1. A schematic microstructure of a two-phase system with second phase particles dispersed in a matrix phase. The orientation field variables η_1, ..., η_j represent different crystallographic orientations of the second phase grains in space. All orientation fields are zero in liquid or disordered (matrix) phase. The equilibrium compositions or solubilities are C_α for the matrix phase and C_β for the second phase respectively.

assume values ranging from -1.0 to 1.0. All orientation field variables are zero in the matrix phase, which simulates the liquid or disordered phase. $C(r)$ is the composition field which takes the value of C_α within the matrix phase and C_β within a second phase grain. $C(r)$ has intermediate values between C_α and C_β at the interfacial region between the matrix phase and a second phase grain.

The total free energy of an inhomogeneous system can be written as:

$$F = \int \left[f_0(C(r); \eta_1(r), \eta_2(r), ..., \eta_p(r)) \right. \tag{1}$$

$$\left. + \frac{\kappa_C}{2}(\nabla C(r))^2 + \sum_{i=1}^{p} \frac{\kappa_i}{2}(\nabla \eta_i(r))^2 \right] d^3 r$$

where ∇C and $\nabla \eta_i$ are gradients of concentration and orientation fields, κ_C and κ_i are the corresponding gradient energy coefficients, and f_0 is the local free energy density which, in this work, is assumed to be,

$$f_0 = f_1(C) + \sum_{i=1}^{p} f_2(C,\eta_i) + \sum_{i=1}^{p}\sum_{j \neq i}^{p} f_3(\eta_i,\eta_j) \tag{2}$$

where

$$f_1(C) = -(A/2)(C-C_m)^2 + (B/4)(C-C_m)^4$$
$$\quad + (D_\alpha/4)(C-C_\alpha)^4 + (D_\beta/4)(C-C_\beta)^4$$

$$f_2(C,\eta_i) = -(\gamma/2)(C-C_\alpha)^2(\eta_i)^2 + (\delta/4)(\eta_i)^4$$

$$f_3(\eta_i,\eta_j) = (\varepsilon_{ij}/2)(\eta_i)^2(\eta_j)^2$$

where C_α and C_β are the solubilities in the matrix phase and the second phase respectively, $C_m = (C_\alpha + C_\beta)/2$, A, B, D_α, D_β, γ, δ, and ε_{ij} are phenomenological parameters. The parameters are chosen in such a way that f_o has $2p$ degenerate minima with equal depth located at $(\eta_1,\eta_2,...,\eta_p) = (1,0,...,0), (0,1,...,0), ..., (0,0,...,1)$ at the equilibrium concentration C_β. This requirement ensures that each point in space can only belong to a grain with a given orientation of a given phase.

This formulation guarantees that, when two particles with different orientations are in contact with each other, a grain boundary forms. Two particles will coalesce when they have the same orientation, which also happens in real systems. The difference is that there are an infinite number of orientations in a real system and only a finite number of order parameters can be used in a simulation. It has been shown [34–37] that, if a large number of order parameters (more then 30) are used in simulations, the kinetics will converge to a value independent of the number of orientations.

It should be pointed out that, in this paper, we only study the coarsening of particles after the initial phase transformation that creates the two-phase mixtures. The driving force for particle coarsening is the minimization of total surface energy (grain boundary energy and interfacial energy). Therefore, as long as the correct grain boundary and interfacial energies can be obtained, the exact form of the free energy density (f_0) is not an issue. Free energy density (f_0) determines the driving force for the phase transformation.

The energy of a planar grain boundary, σ_{gb}, between a grain of orientation i and another grain of orientation j for two second phase grains, can be written as follows,

$$\sigma_{\text{gb}} = \int_{-\infty}^{+\infty} \left[\Delta f(\eta_i,\eta_j,C) + \frac{\kappa_C}{2}\left(\frac{\mathrm{d}C}{\mathrm{d}x}\right)^2 \right. \tag{3}$$

$$\left. + \frac{\kappa_i}{2}\left(\frac{\mathrm{d}\eta_i}{\mathrm{d}x}\right)^2 + \frac{\kappa_j}{2}\left(\frac{\mathrm{d}\eta_j}{\mathrm{d}x}\right)^2 \right] \mathrm{d}x$$

in which

$$\Delta f(\eta_i,\eta_j,C) = f_0(\eta_i,\eta_j,C) - f_0(\eta_{i,\text{e}},\eta_{j,\text{e}},C_\beta) - (C \tag{4}$$

$$- C_\beta)\left(\frac{\partial f_0}{\partial C}\right)_{\eta_{i,\text{e}},\eta_{j,\text{e}},C_\beta}$$

where $f_0(\eta_{i,\text{e}},\eta_{j,\text{e}},C_\beta)$ represents the free energy density minimized with respect to η_i and η_j at the equilibrium composition of the second phase C_β. Similarly, the interphase boundary energy between the matrix phase and a second phase grain with orientation i can be defined.

In the present model, the evolution kinetics of these field variables are described by the generalized time-dependent Ginzburg–Landau (TDGL) and Cahn–Hilliard equations:

$$\frac{\mathrm{d}\eta_i(r,t)}{\mathrm{d}t} = -L_i\frac{\delta F}{\delta\eta_i(r,t)}, \quad i = 1,2,...,p, \tag{5a}$$

$$\frac{\mathrm{d}C(r,t)}{\mathrm{d}t} = \nabla\left\{D\nabla\left[\frac{\delta F}{\delta C(r,t)}\right]\right\}, \tag{5b}$$

where L_i and D are kinetic coefficients related to grain boundary mobilities and atomic diffusion coefficients, t is time, and F is the total free energy given in Eq. (1). The difference between kinetic equations for orientation field variables $\eta_i(r)$ and concentration field $C(r)$ comes from the fact that $C(r)$ is a conserved field, due to the requirement of mass conservation, and the orientation fields are non-conserved variables.

3. Simulation results and discussions

3.1. Microstructural evolution and scaling

To study Ostwald ripening, we chose a set of 30 orientation variables and a concentration field to characterize the microstructures. A 2-D 512×512 square system was employed. The

phenomenological parameters were chosen such that the liquid, or matrix, phase totally wets the solid, or coarsening, phase, i.e., the ratio of grain boundary energy to interfacial energy is larger than 2.0. We assumed the following phenomenological parameters in Eqs. (1)–(4): $C_\alpha = 0.05$, $C_\beta = 0.95$, $C_m = (C_\alpha + C_\beta)/2 = 0.5$, $A = 2.0$, $B = A/(C_\beta - C_m)^2$, $\gamma = 2/(C_\beta - C_\alpha)^2$, $\delta = 1.0$, $D_\alpha = D_\beta = \gamma/\delta^2$, $\varepsilon_{ij} = 3.0$. The gradient coefficients were chosen as: $\kappa_i = \kappa_j = \kappa_C = 2.0$. These parameters give an energetic ratio $\sigma_{\text{gb}}/\sigma_{\text{in}} = 2.14$, which satisfies the total wetting condition. The kinetic equations were discretized using centered finite differences and integrated in time using an explicit method. The grid size along both Cartesian coordinate axes, Δx, was chosen to be 2.0, and the time step for integration, $\Delta t = 0.1$. Periodic boundary conditions were applied. The diffusivities and mobilities were assumed to be the same for both phases.

Computer simulations were started from a liquid or disordered phase, i.e., a phase with small random values for all field variables (± 0.001) and the average concentration for the composition field with thermal noise. This ensures the desired volume fractions. After the quench, grains of the coarsening phase will spontaneously nucleate from the liquid or disordered phase. The nucleation process was completed roughly within first 1500 time steps. Allowing enough time for the system to reach the steady state or as close as we could reach in these calculations (after the first 5000 time steps), the kinetic data for Ostwald ripening and size distributions were extracted from the simulated microstructures. At time step 5000, there are about 600 grains or particles in the 25% coarsening phase system and about 700 grains in the high volume fraction systems. The simulations were stopped when there were about 100 grains left in the 25% volume fraction system and about 200 left in the high volume fraction systems.

The temporal evolution of the microstructures with 25%, 50%, 75%, and 90% volume fractions of second phase is shown in Figs. 2–5, respectively. In these microstructures, the bright phase is the coarsening, or solid, phase, and the dark phase represents the matrix phase. It can be seen that at
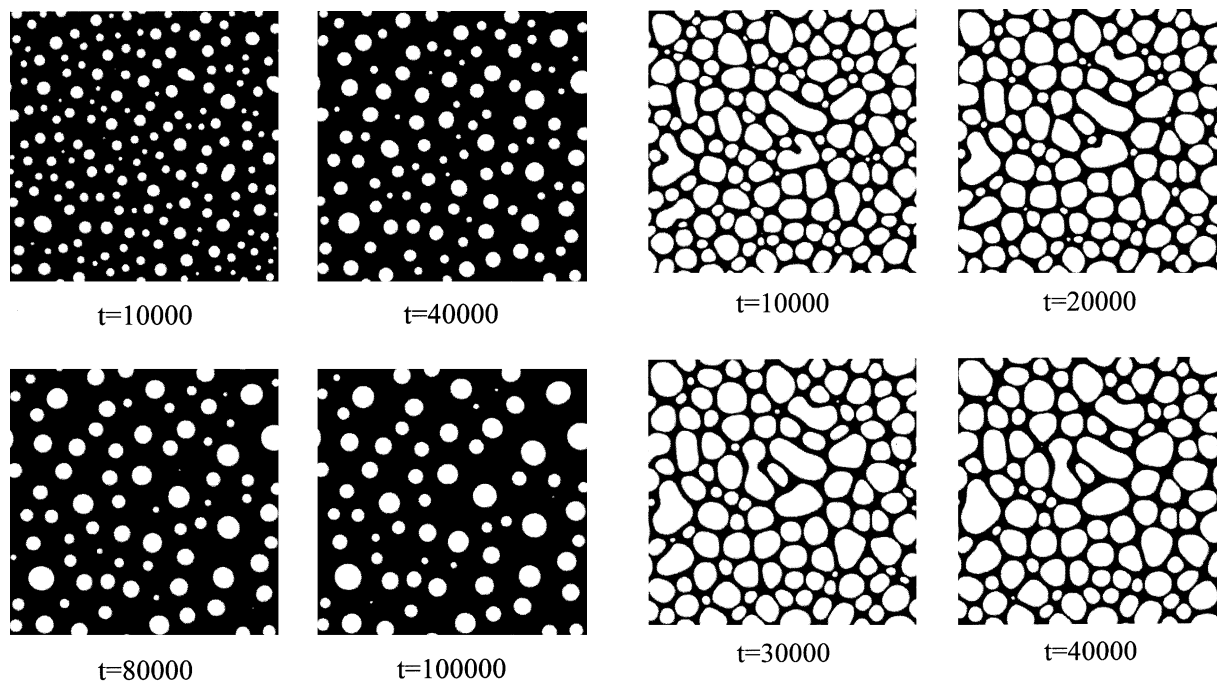
Fig. 2. Microstructural evolution of Ostwald ripening in 2-D with 25% coarsening phase. The system size is 512×512. The initial microstructure is a liquid. After nucleation, there are about 600 particles in this system at the 5000 time step.
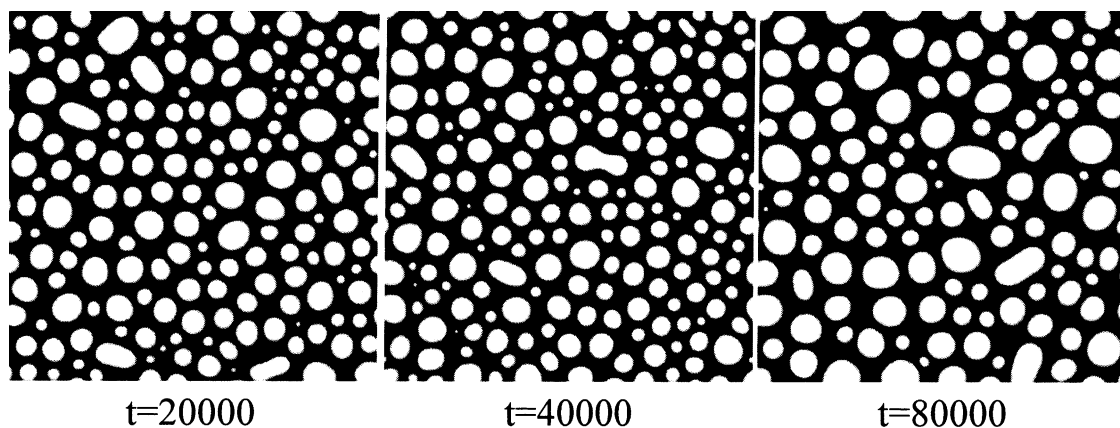

Fig. 4. Microstructural evolution of Ostwald ripening in 2-D with 75% coarsening phase. The system size is 512×512. The initial microstructure is a liquid. After nucleation, there are about 650 particles in this system at the 5000 time step.

Fig. 3. Microstructural evolution of Ostwald ripening in 2-D with 50% coarsening phase. The system size is 512×512. The initial microstructure is a liquid. After nucleation, there are about 750 particles in this system at the 5000 time step.

low volume fraction (25%), the coarsening grains are almost perfect circles and the coarsening is solely controlled by the interparticle diffusion through the matrix phase. At 50% of the coarsen-

ing phase, particle coalescence is observed, which is the result of a finite number of orientation variables employed in the simulations, and most of the grains are still nearly circular. However, at 75%
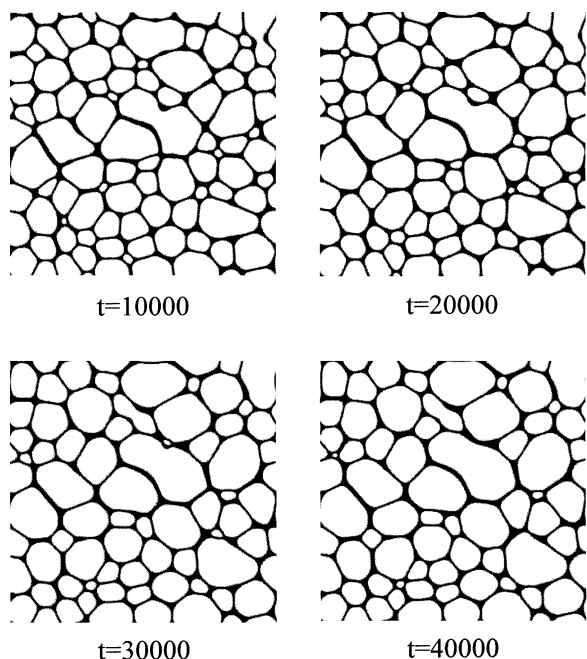
Fig. 5. Microstructural evolution of Ostwald ripening in 2-D with 90% coarsening phase. The system size is 512×512. The initial microstructure is a liquid. After nucleation, there are about 650 particles in this system at the 5000 time step.

volume fraction, shape accommodation becomes apparent and the particle shapes start to depart from circular shapes. The microstructures with volume fractions larger than 90% are comprised of particles with flattened sides, curved edges and rounded vertices or corners. In all cases, the coarsening particles are wetted by the matrix phase as a result of our choice of the gradient energy coefficients.

A common method used to determine whether a system has reached the scaling regime is to examine the normalized structural function $S(k, t)$ [41–43], which is the Fourier transform of the spatial correlation function. It is suggested that the normalized structural function can be written as $s(k,t) = \kappa(t)^d F(x,t)$, where k is the wave vector, d dimensions, $x = k/\kappa(t)$, t the time, $\kappa(t)$ a time-dependent length scale which behaves as $\kappa(t) \sim t^n$ for positive n. $F(x, t)$ is called the scaling function. In the scaling regime, $F(x,t) = F(x)$, which is independent of time.

Therefore, the dynamical scaling of a system can

be determined by calculating the scaling function of the system. If the shape of the scaling function does not change significantly with time, it means that the system has reached the scaling state or steady state. Following the formulations of Lebowitz et al. [37], the structure functions and its scaled version are calculated. Fig. 6 shows an example of the calculated scaling function for the 90% coarsening phase system at different time steps. It is clear that scaling functions are invariant with time, indicating that over the time scale of our calculations, the system may have reached the steady state. It should be pointed out that due to the limited system size and limited number of time steps in our simulations, Fig. 6 is not a rigorous proof that the system has reached the scaling regime. It is possible that the system evolves very slowly to the scaling regime, and the statistics are not sufficiently accurate to distinguish potentially small variations in the scaling functions. The scaling functions in other volume fractions are similar to Fig. 6.
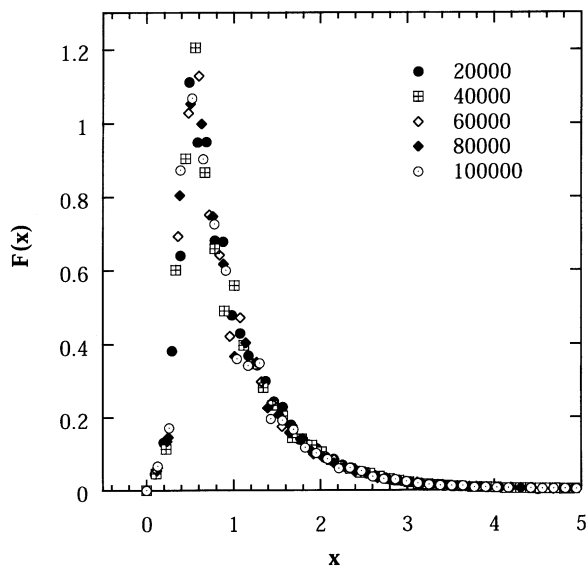

Fig. 6. Relations of the scaling function $F(x, t)$ with the normalized wave number x ($x = k/\kappa(t)$) in the reciprocal space at different time steps in 90% coarsening phase system. Time step=20,000, 40,000, 60,000, 80,000, and 100,000.

3.2. Kinetics of Ostwald ripening

The time dependence of the average grain size in systems with 25% and 90% of the coarsening phase are shown in Figs. 7 and 8. In these plots, the solid lines are the non-linear fits to the power growth law $R_t^m - R_0^m = kt$ with three variables m, k and R_0. It is found that these data fit the power growth law very well with $m = 3$ in all cases, even for the very high volume fraction of coarsening phase (90%). Thus even in systems with 90% volume fraction the coarsening process is not well described by $m = 1/2$, which would be expected in the limit of very high volume fractions. It is clear that the shape accommodation of particles will not affect the growth exponent m as long as the system is in the scaling regime. Even though the growth exponent is independent of the volume fraction of the coarsening phase, the kinetic coefficient k is strongly volume-fraction dependent.

The dependence of the kinetic coefficient k on the volume fraction of the coarsening phase is shown in Fig. 9. At 25% coarsening phase, the kinetic coefficient k is 0.833, while at 90% coarsening
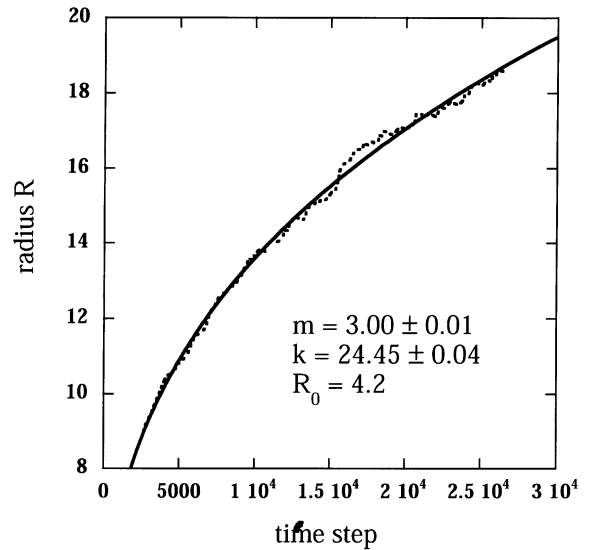
Fig. 8. Time dependence of the average grain size of the coarsening phase in the 90% coarsening phase system. The dots are the measured data from simulated microstructures. The solid line is a non-linear fit to the power growth law $R_t^m - R_0^m = kt$ with three variables m, k and R_0.
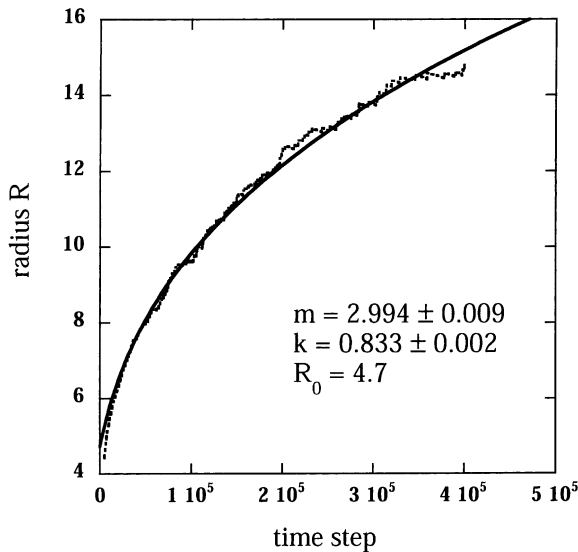
The text inside Fig. 8:
m = 3.00 ± 0.01
k = 24.45 ± 0.04
$R_0 = 4.2$

Fig. 7. Time dependence of the average grain size of the coarsening phase in the 25% coarsening phase system. The dots are the measured data from simulated microstructures. The solid line is a non-linear fit to the power growth law $R_t^m - R_0^m = kt$ with three variables m, k and R_0.

The text inside Fig. 7:
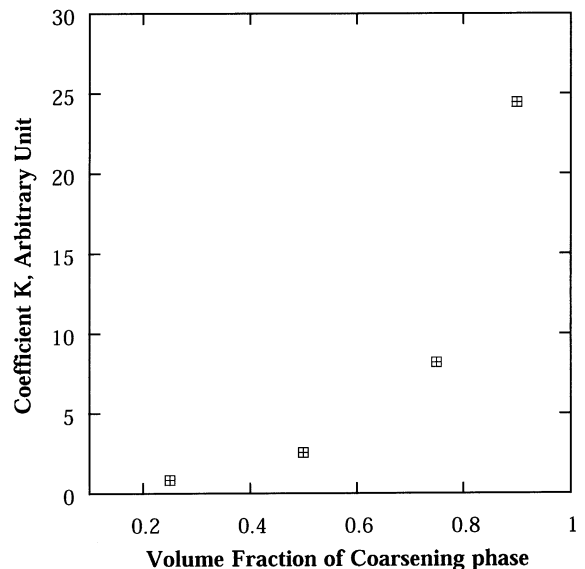m = 2.994 ± 0.009
k = 0.833 ± 0.002
$R_0 = 4.7$

Fig. 9. Dependence of the kinetic coefficient k on the volume fraction of the coarsening phase.

phase, the coefficient increases to 24.45 that is about 30 times higher than that in the 25% system. The rapid increase in the kinetic coefficient k can be attributed to the dramatic decrease of the diffusion distance of atoms in the matrix phase as the volume fraction of coarsening phase increases. At low volume fraction (25%), the typical diffusion distance is the mean spacing between particles, which is much larger than the grain boundary thickness. At 90% coarsening phase, it can be seen from microstructures (Fig. 5) that the typical diffusion distance between grains becomes comparable with the grain boundary width, which will greatly enhance the coarsening kinetics but, as mentioned above, not change the temporal exponent. The rapid increase in k at high volume fraction is qualitatively similar to that obtained from experiments using solid–liquid mixtures in the Fe–Cu, Co–Cu, Pb–Sn, Sn–Pb systems [3].

3.3. Size distributions

Examples of size distributions at different times in systems with 25% and 90% coarsening phase are shown in Figs. 10 and 11, respectively. It is

Fig. 11. Time dependence of grain size distributions in 90% coarsening phase system. Time step=5000, 7500, 10,000, 12,500, 15,000. There are about 500 grains at the 5000 time step and 300 grains at the 15,000 time step.

clear that the shapes of size distributions in all systems does not vary significantly with time, indicating the system evolves very slowly to the true scaling regime or the system is very close to the scaling regime. However, the shapes of size distributions between different volume fractions are different. The dependence of the shape of size distributions on the volume fraction is given in Fig. 12. In this plot, the dots represent the average data of size distributions at different volume fractions, and the lines are the smooth fits to those data. For a direct comparison, all size distributions at different volume fractions were normalized to satisfy the relation $\Sigma\rho(x)\,dx = 1$, where $\rho(x)$ is the size distribution, and $x = R/\langle R\rangle$. As the volume fraction of the coarsening phase increases, the size distribution broadens and the peak of the size distribution decreases. Fig. 12 also shows that in the low volume fraction regime (25%), the size distribution skews to the left side and becomes more symmetric at 50%. To quantitatively study the skewness of the size distributions, the skewness was calculated for different volume fractions, as shown in Fig. 13, in which the skewness is defined as $\mu_3/\mu_2^{3/2}$, where μ_m is the mth moment of the size distribution. A
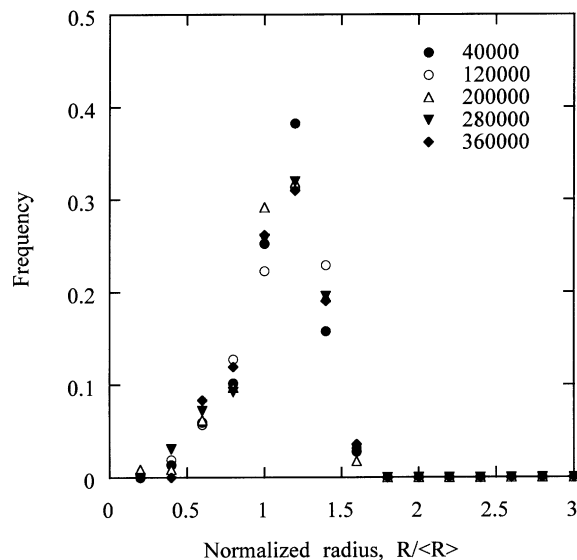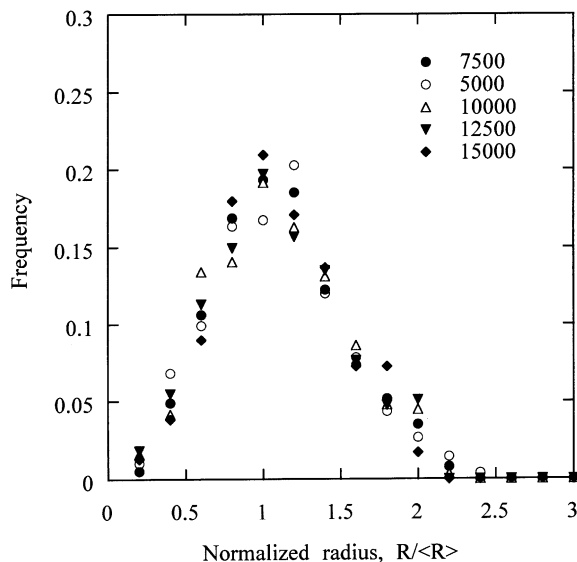

Fig. 10. The time dependence of grain size distributions in 25% coarsening phase system. Time step=40,000, 120,000, 200,000, 280,000, 360,000. There are about 300 grains at the 40,000 time step and 100 grains at the 360,000 time step.
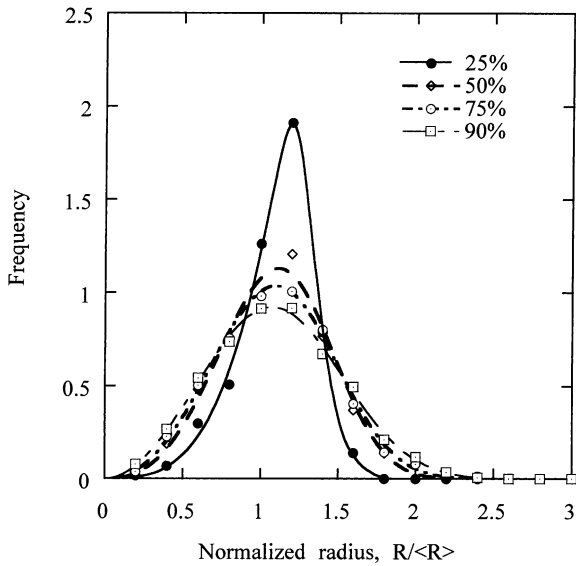
Fig. 12. Dependence of grain size distributions on the volume fraction of coarsening phase. Dots represent the average data of size distributions at different volume fractions and lines are the smooth fits to those data.

positive skewness means the distribution has a longer tail to the right of the mean value than to the left. If the reverse is true, skewness is negative. It can be seen that at 25% volume fraction the skewness is negative, i.e., skewed to the left, and that it continuously changes toward positive values as the volume fraction increases. In the high volume fraction regime, the size distributions skew to the right in contrast to the low volume fraction regime. Most theories, on the other hand, predict that skewness increases with the volume fraction of coarsening phase, but does not change sign. It should be noted, however, that there are very few theories that attempt to predict the particle size distributions at volume fractions in excess of 70% and thus this change in the sign of the skewness may be primarily a result of the volume fractions employed in our computer simulations.

Another important characteristic of size distributions is the so-called kurtosis, the degree of peakedness of distributions. The kurtosis or excess kurtosis is defined as μ_4/μ_2^2-3, which is the relative sharpness compared to the normal distribution. The dependence of kurtosis of the size distributions on the volume fraction is shown in Fig. 14. At low volume fraction (25%), the kurtosis is positive and
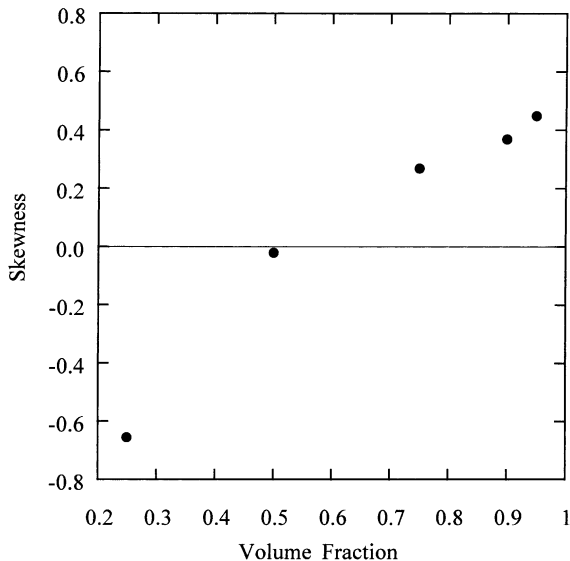

Fig. 13. Dependence of the skewness of size distributions on the volume fractions of the coarsening phase.
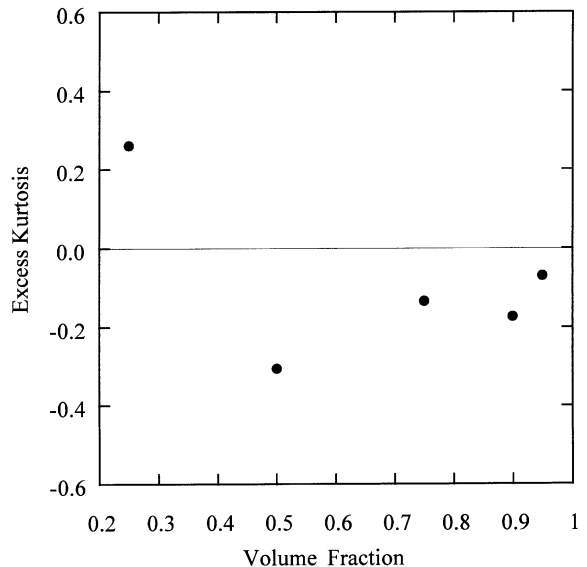

Fig. 14. Dependence of the kurtosis of size distributions on the volume fractions of the coarsening phase.

more peaked than the normal distribution. A rapid decrease of peakedness is observed from 25% to 50% of the coarsening phase, and the kurtosis is negative for the 50% case, indicating that it is more flattened than the normal distribution. In this volume fraction regime ($<$50%), the trend of kurtosis as a function of volume fraction agrees with the prediction of analytical theories, i.e., the peak of size distributions becomes more flattened (decreasing kurtosis) with increasing volume fraction. However, in the high volume fraction regime ($>$50%), the kurtosis increases with increasing volume fraction, i.e., the size distribution becomes more peaked as it continuously skews to the right side.

Similar behaviors for skewness and kurtosis in the high volume fraction regime have also been found in Monte Carlo simulations by Tikare [44]. However, since the Monte Carlo simulations were only performed in the higher volume fraction regime ($>$40%), there is no reported continuous change of skewness from a large negative value (strongly skewed to the left) to a large positive value (strongly skewed to the right), and the significant decrease of kurtosis from positive to negative in the low volume fraction regime. Both Monte Carlo and current simulations showed that in the high volume fraction regime size distributions skew to the right and peakedness increases with increasing volume fraction of the coarsening phase. Davies et al. [45] predicted the change of skewness from negative to positive with increasing volume fraction in 3-D, by taking into account the encounter or coalescence of particles and modifying the continuity equation of LSW theory. However, the coalescence of particles was explicitly prevented in Monte Carlo simulations while in the current simulations the coalescence did occur. Since both simulations predicted similar behaviors for skewness and kurtosis in the high volume fraction regime, the coalescence may not be the controlling factor that determines the volume-fraction dependences of skewness and kurtosis. The factors that may affect their volume-fraction dependences should include the spatial correlations of particles and shape accommodation in the high volume fraction regime, which affect the local driving force and local concentration gradient and in turn may

influence the shape of size distributions. A second possibility is that the evolution of the particle size distribution towards its asymptotic shape may be extremely slow at high volume fractions, and thus the observed skewness would disappear if the system were allowed to coarsen longer [33].

The size distribution for the 25% coarsening phase system predicted by the current simulation is compared with the result for 21% coarsening phase obtained by Chakrabarti et al. [17] through numerically solving the Cahn–Hilliard equation, as shown in Fig. 15. It can be seen that these two results are almost identical. As a matter of fact, the current model will reduce to the Cahn–Hilliard equation if no orientation field variables are involved. However, the Cahn–Hilliard equation itself cannot be employed to study Ostwald ripening in the high volume fraction regime since an interconnected microstructure will be formed when the volume fraction is larger than about 40%. At the low fraction regime, the current model and numerical solution of the Cahn–Hilliard equation are equivalent.

Due to the lack of experimental and theoretical results in 2-D for the high volume fraction regime, the current simulation result of 50% volume frac-
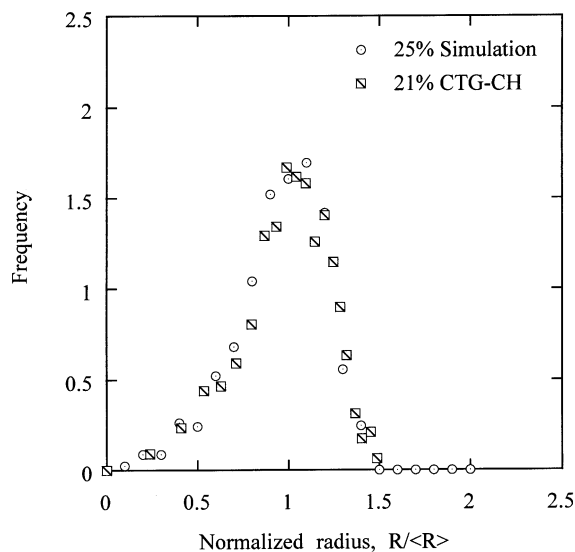

Fig. 15. Comparison of the size distribution of the present result in 25% coarsening phase system with the result for 21% coarsening phase system obtained by Chakrabarti et al. [17] through numerical solving the Cahn–Hilliard equation.

tion is compared with the thin-film experimental result of 40% [24] and the theoretical prediction at 40% by Marqusee [16], as shown in Fig. 16. To make a direct comparison, these distributions were normalized to satisfy the relation $\Sigma\rho(x)\,\mathrm{d}x = 1$. It is clear that the shape of the distribution obtained from the current simulation is in good agreement with the shape obtained from 2-D experiment results, except at the large size regime. The frequencies of large size particles in the current simulation with 50% coarsening phase are higher than those obtained from experiments with a volume fraction of 40% coarsening phase. This difference could come from the higher volume fraction in the simulated system, and from the fact that some coalescence is observed in the simulated 50% system. This difference has been found to be a signature of a transient coarsening process [33]. It was found that very long coarsening times are required for the largest growing particles to decrease their size relative to the average and thus decrease the magnitude of the frequency at large $R/\langle R\rangle$. It is thus possible that the calculated scaled distributions are not completely in steady state.

3.4. Effect of partial wetting

In the above simulations and all other theories a total wetting energetic condition was assumed. However, in many practical systems or solid–liquid two-phase alloys, the liquid, or matrix, phase only partially wets the solid phase or coarsening phase. The partial wetting energetic condition will result in direct contact between particles of the coarsening phase, which changes the local concentration distribution and local curvatures. Therefore, it is necessary to examine if the wetting condition will affect the coarsening kinetics of Ostwald ripening.

In this section, a system with 90% of coarsening phase and with the energetic ratio $\sigma_{gb}/\sigma_{in} = 1.85$ was chosen to study the effect of the energetic ratio on coarsening kinetics. The temporal evolution of the microstructure of this system is shown in Fig. 17. It can be seen that microstructures under this energetic condition are quite different from those of total wetting systems. The liquid phase or matrix
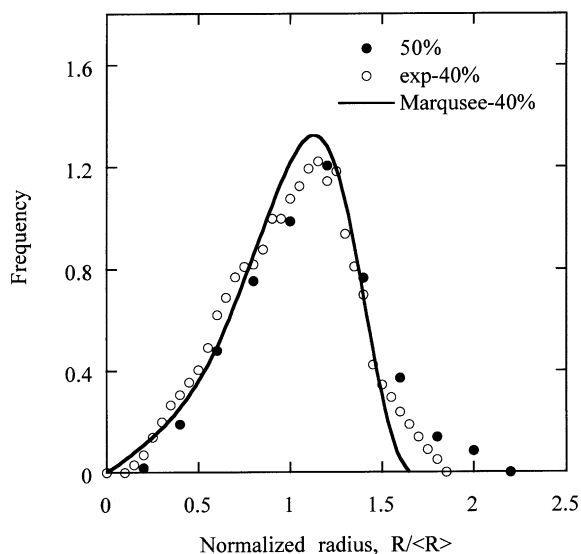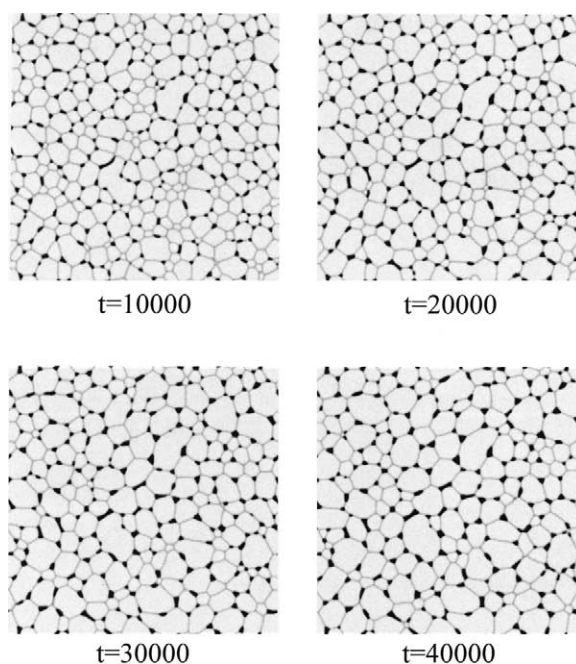

Fig. 16. Comparison of the size distribution of the present result in 50% coarsening phase system with the prediction of Marqusee theory [16] and experimental result [24] for 40% coarsening phase system.

Fig. 17. Microstructural evolution in the partial wetting system with 90% coarsening phase. $\sigma_{gb}/\sigma_{in} = 1.85$. The system size is 512×512. The initial microstructure is a liquid. After nucleation, there are about 580 particles in this system at the 5000 time step.

phase is not continuous anymore and stays at grain boundaries and grain corners of the coarsening phase because of its low volume fraction. The time dependence of the average grain size of the coarsening phase is shown in Fig. 18. It is quite interesting to see that the growth exponent *m* is still 3 for the coarsening phase, which is not affected by the change in wetting conditions and microstructural details. Therefore, as long as Ostwald ripening is the rate controlling process in a two-phase mixture, the growth exponent will not depend on which phase undergoes Ostwald ripening. Because we assume the same diffusivity for both phases, the kinetic coefficient *k* in this partial wetting system is also identical to that of a total wetting system with 90% coarsening phase. However, if the diffusivities are different in the two phases and in the grain boundary regions, a strong dependence of kinetic coefficient *k* on the wetting condition can be expected. The time dependence of size distributions in this system is shown in Fig. 19. These size distributions are approximately self-similar or time-invariant, indicating the system is nearly at the steady state. The shape of these size distri-

Fig. 19.   Time dependence of size distributions in the partial wetting system with 90% coarsening phase. $\sigma_{gb}/\sigma_{in} = 1.85$. Time step=5000, 7500, 10,000, 12,500, 15,000. There are about 450 grains at time step 5000 and 250 grains at time step 15,000.

butions is equivalent to that in the total wetting system with 90% coarsening phase. Hence, under the assumption of both phases having the same diffusivity, the characteristics of Ostwald ripening are not affected by the wetting condition, even though the microstructures are very different in total wetting and partial wetting systems. This is not the case if the diffusivities are different for two phases and in grain boundary regions [46].

4. Summary

The characteristics of Ostwald ripening in a two-phase mixture have been systematically studied over a range of volume fractions of the coarsening phase. It was found that the growth exponent $m = 3$ is independent of the volume fraction of the coarsening phase and the details of the microstructures up to a volume fraction of 90%. The kinetic coefficient *k* increases as the volume fraction of the coarsening phase increases, with a very strong increase above volume fractions of 70%. The simulation predictions agree well with experimental results from different systems. It was shown
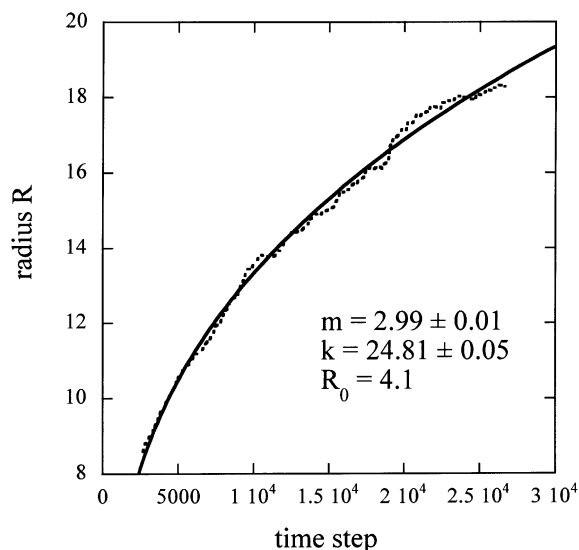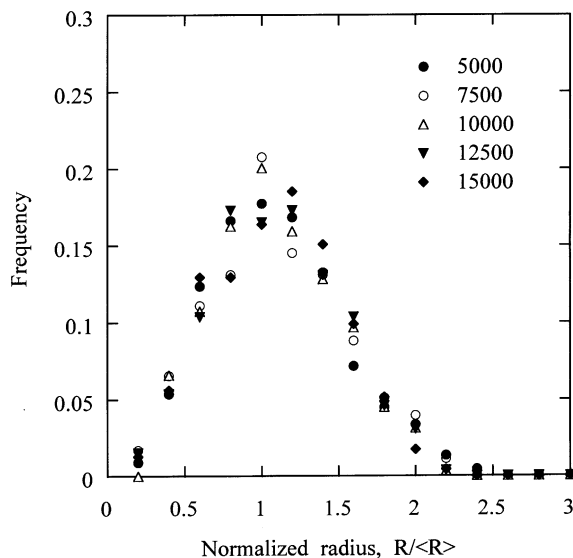

Fig. 18.   Time dependence of the average grain size in the partial wetting system with 90% coarsening phase. $\sigma_{gb}/\sigma_{in} = 1.85$. The dots are the measured data from simulated microstructures. The solid line is a non-linear fit to the power growth law $R_t^m - R_0^m = kt$ with three variables *m*, *k* and R_0.

that the shape of size distributions changes dramatically with increasing volume fraction of the coarsening phase. The skewness continuously changes from negative to positive while the kurtosis decreases in the low fraction regime and increases in the high volume fraction regime. The wetting of a second phase will not affect the coarsening exponent under the conditions that two phases and grain boundary have the same diffusion coefficient or mobility, and the volume diffusion is the controlling mechanism for diffusion.

Acknowledgements

References

[1] Lifshitz M, Slyozov VV. J Phys Chem Solids 1961;19:35.
[2] Wagner C. Z Elektrochem 1961;65:581.
[3] Voorhees PW. Annu Rev Mater Sci 1992;22:197 and references therein.
[4] Ardell J. Acta Metall 1972;20:61.
[5] Tsumuraya K, Miyata Y. Acta Metall 1983;31:437.
[6] Brailsford D, Wynblatt P. Acta Metall 1979;27:489.
[7] Voorhees PW, Glicksman ME. Acta Metall 1984;32:2013.
[8] Yao JH, Elder KR, Guo H, Grant M. Phys Rev B 1993;47:14110.
[9] Marqusee JA, Ross J. J Chem Phys 1984;80:536.
[10] Dehoff RT. Acta Metall 1991;39:2349.
[11] Akaiwa N, Voorhees PW. Phys Rev E 1994;49:3860.
[12] Fang Z, Patterson BR, Turner ME. Acta Metall 1992;40:713.
[13] Beenakker CWJ. Phys Rev A 1986;33:4482.
[14] Rogers TM, Desai RC. Phys Rev B 1989;39:11956.
[15] Ardell J. Phys Rev B 1990;41:2554.
[16] Chakrabati A, Toral R, Gunton JD. Phys Rev E 1993;47:3025.
[17] Marqusee JA. J Chem Phys 1984;81:976.
[18] Zheng Q, Gunton JD. Phys Rev A 1989;39:4848.
[19] Yao JH, Elder KR, Guo H, Grant M. Phys Rev B 1992;45:8173.
[20] Akaiwa N, Meiron DI. Phys Rev E 1996;54:R13.
[21] Voorhees PW, McFadden GB, Boisvert RF, Meiron DI. Numerical simulation of morphological development during Ostwald ripening. Acta Metall 1988;36:207.
[22] Kingery WD. J Appl Phys 1959;30:301.
[23] Johnson WC, Abinandanan TA, Voorhees PW. Acta Metall 1990;38:134.
[24] Hardy SC, Voorhees PW. Metall Trans A 1988;19:2713.
[25] Niemi N, Courtney TH. J Mater Sci 1981;16:226.
[26] Kang H, Yoon DN. Metall Trans A 1981;12:65.
[27] Krichevsky O, Stavans J. Phys Rev E 1995;52:1818.
[28] Wong J. J Appl Phys 1980;51:4453.
[29] Smith F. Acta Metall 1967;15:1867.
[30] Yang SC, German RM. J Am Ceram Soc 1991;74:3085.
[31] Mani SS, Fradkov VE, Glicksman ME. In: Proceedings of ASM/TMS International Meeting, Pittsburgh (PA), 1994.
[32] Krichevsky O, Stavans J. Phys Rev Lett 1993;70:1473.
[33] Snyder VA, Alkemper J, Voorhees PW. Acta Mater 2001;49:699.
[34] Fan D, Chen L-Q. Acta Mater 1997;45(2):611.
[35] Fan D, Chen L-Q. Acta Mater 1997;45(3):1115.
[36] Fan D, Chen L-Q. Acta Mater 1997;45(8):3297.
[37] Chen L-Q, Fan D. J Am Ceram Soc 1996;79:1163.
[38] Fan D, Chen L-Q. Acta Mater 1997;45(10):4145.
[39] Fan D, Chen L-Q. J Am Ceram Soc 1997;80(7):1773.
[40] Fan D, Chen L-Q, Chen SP, Voorhees PW. Comput Mater Sci 1998;9:329.
[41] Lebowitz JL, Marro J, Kalos MH. Acta Metall 1982;30:297.
[42] Oona Y, Puri S. Phys Rev Lett 1987;58:836.
[43] Enomoto Y, Kato R. J Phys.: Condens Matter 1990;2:9215.
[44] Tikare V. Numerical simulation of grain growth in liquid phase sintered materials. PhD thesis, Case Western Reserve University, 1994.
[45] Davies KL, Nash P, Stevens RN. Acta Metall 1980;28:179.
[46] Eggleston JJ, Voorhees PW. In preparation.